Quinn A. Besford, Holger Merlitz, Simon Schubotz, Huaisong Yong, Soosang Chae, Max J. Schnepf, Alessia C. G. Weiss, Günter K. Auernhammer, Jens-Uwe Sommer, Petra Uhlmann, Andreas Fery

Mechanofluorescent Polymer Brush Surfaces that Spatially Resolve Surface Solvation

Erstveröffentlichung in / First published in:

ACS Nano. 2022, 16 (2), S. S. 3383–3393. ACS Publications. ISSN 1936-086X.

DOI: https://doi.org/10.1021/acsnano.2c00277

Final edited form was published in "ACS nano". 16 (2), S. 3383–3393. ISSN: 1936-086X.
https://doi.org/10.1021/acsnano.2c00277

Mechanofluorescent Polymer Brush Surfaces that Spatially Resolve Surface Solvation

Quinn A. Besford,* Holger Merlitz, Simon Schubotz, Huaisong Yong, Soosang Chae, Max J. Schnepf, Alessia C. G. Weiss, Günter K. Auernhammer, Jens-Uwe Sommer, Petra Uhlmann, and Andreas Fery*

ABSTRACT: **Polymer brushes, consisting of densely end tethered polymers to a surface, can exhibit rapid and sharp conformational transitions due to specific stimuli, which offer intriguing possibilities for surface based sensing of the stimuli. The key toward unlocking these possibilities is the development of methods to readily transduce signals from polymer conformational changes. Herein, we report on single fluorophore integrated ultrathin (<40 nm) polymer brush surfaces that exhibit changing fluorescence properties based on polymer conformation. The basis of our methods is the change in occupied volume as the polymer brush undergoes a collapse transition, which enhances the effective concentration and aggregation of the integrated fluorophores, leading to a self quenching of the fluorophores' fluorescence and thereby reduced fluorescence lifetimes. By using fluorescence lifetime imaging microscopy, we reveal spatial details on polymer brush conformational transitions across complex interfaces, including at the air−water−solid interface and at the interface of immiscible liquids that solvate the surface. Furthermore, our method identifies the swelling of polymer brushes from outside of a direct droplet (*i.e.*, the polymer phase with vapor above), which is controlled by humidity. These solvation sensitive surfaces offer a strong potential for surface based sensing of stimuli induced phase transitions of polymer brushes with spatially resolved output in high resolution.**

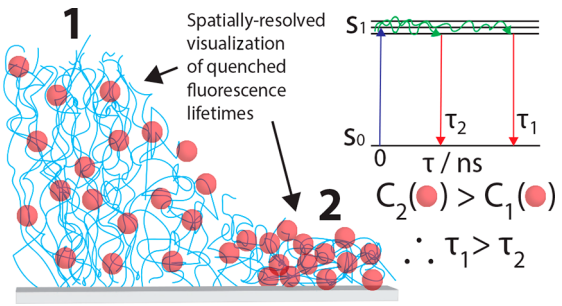

KEYWORDS: *polymer brushes, mechanofluorescence, fluorescence lifetime imaging microscopy, poly(N isopropylacrylamide), co nonsolvency effects, droplet wetting*

Polymer brushes are ubiquitous for use in applications ranging from substrates for selective bioadhesion[1,2] to switchable surfaces for adhesion and wettability[3,4] and real time surface based sensing materials.[5] For example, the swelling of polymer brushes can modulate the shape, cytoskeleton distribution, and growth of cells,[6] strongly influence the repellency against oil,[7] and allow for surface based sensing of vapor.[8] These broad applications, in large part, stem from an ability to exhibit rapid switching transitions between surface properties (*e.g.*, adhesion) and hydration properties (*e.g.*, swelling) from both liquid and vapor. The root cause of this functionality is strong cooperative action between highly dense end tethered polymer chains, where the conformation of a single chain is dependent on the conformation of its neighbors. Certain stimuli can cause phase transitions of the polymer chains, leading to rapid and communal switching in polymer conformation from the extremes of being fully swollen to collapsed. Such stimuli are strongly dependent on the chemistry of the polymer itself but can include pH,[9] temperature,[10] solvent,[11] and mechanical force,[12] meaning that polymer brush surfaces can be leveraged towards multimodal surface based sensing materials if the transitions in conformation can be readily identified. Therefore, understanding how polymer brush transitions evolve spatially and at complex interfaces may allow for the development of greater surface based sensing materials, for example, for understanding biological adhesion processes.

From a physical perspective, a key interface of interest is that at the boundary of a liquid droplet on a polymer brush. These interfaces can exhibit a restructuring of the exposed polymer chains due to the nature of the liquid, ultimately leading to surface memory effects,[13] and they can play a role in adaptive repellency toward specific liquids/solutes (*i.e.*, fouling)[7] and the adsorption of specific liquids into polymer layers to produce fiction free droplet motion.[14] However, the conformation and swelling of polymer brushes at these interfaces

Received: January 10, 2022
Accepted: January 27, 2022
Published: February 3, 2022

Final edited form was published in "ACS nano". 16 (2), S. 3383–3393. ISSN: 1936-086X.
https://doi.org/10.1021/acsnano.2c00277

Scheme 1. Schematic for the Synthesis of the Rhodamine B (Rhod B) Monomer (Rhod B–HEA) (Red Spheres) (A) and Its Incorporation into a Random Copolymer with NIPAM (Blue Spheres) Achieved *via* RAFT (B)[a]

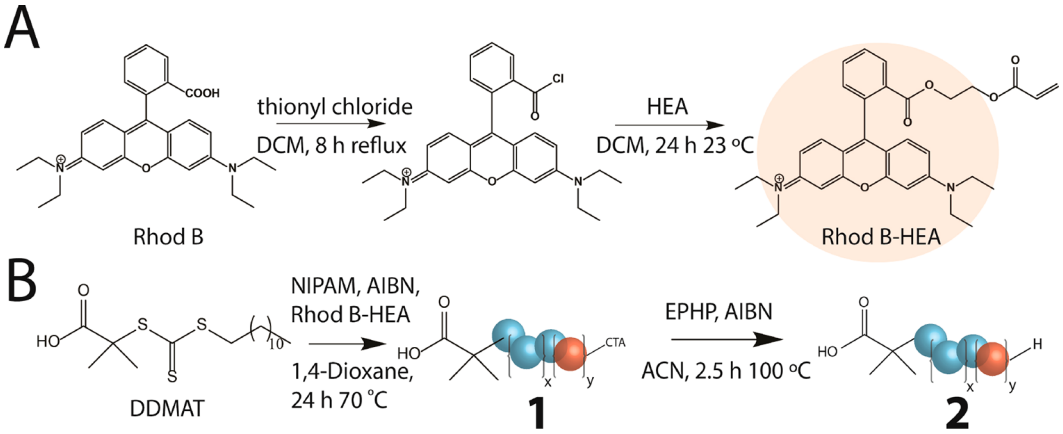

[a]DCE, dichloroethane; DCM, dichloromethane; HEA, 2 hydroxyethylacrylate; NIPAM, *N* isopropylacrylamide; AIBN, azobisisobutyronitrile; DDMAT, 2 (dodecylthiocarbonothioylthio) 2 methylpropionic acid; CTA, chain transfer agent; EPHP, *N* ethylpiperidine hypophosphite; ACN, acetonitrile.

remains tantalizingly difficult to analyze quickly across phase boundaries (*i.e.*, from dry to solvated polymer chains under a droplet).[15] Conventionally, polymer brush conformation has been probed by atomic force microscopy (AFM), using a colloidal probe to identify changes in surface properties[16] or in tapping mode to identify brush height[17] or alternatively using spectroscopic ellipsometry.[11] These methods, however, suffer from drawbacks in terms of acquisition time, spatial resolution, and an inability to be used in complex architectures (*i.e.*, surfaces that depart from planar or spherical (AFM) substrates). In overcoming these limitations, systems have been developed to extrapolate signals from changing polymer conformation by incorporating plasmonic nanoparticles into the brush architecture, which allow for UV–visible spectroscopy (UV–vis) and naked eye[18] monitoring of plasmonic band shifts due to particle proximity in the brush. Other optical motifs can be incorporated within the polymer brush, including luminescent nanocrystals that exhibit proximity based quenching[19] or aggregation induced emission (AIE).[20] The latter has typically been used for nanoparticle anchored polymer brush formulations.[21] Alternatively, molecular fluorophores have been incorporated onto the polymer chain ends, achieved through click chemistry,[22−24] where the fluorescence intensity of the resulting fluorophore tethered brushes can be correlated to the brush height, as the collapse of the brush is thought to lead to aggregation induced quenching of the fluorescence intensity. This aggregation induced quenching is specific to each fluorophore; as elsewhere, it has been shown that acrylonitrile based polymer brushes exhibit AIE in the collapsed state.[25] These optical read out polymer brush systems have not been applied in high resolution and spatially resolved investigations of brush transitions at liquid droplet–surface interfaces to the best of our knowledge.

Recently, Förster resonance energy transfer (FRET) integrated polymer brushes as optical sensors of brush conformation were reported,[26] which were based on the separation between donor and acceptor fluorophores in complex diblock random copolymers. These FRET based systems provided spatially resolved output of conformation, for its purpose, albeit with limitations in moving toward more complex systems. Principally, in a polymer brush, a large degree of permanent FRET pairing exists, which dampens the dynamic range of sensing as well as placing limitations in terms of crosstalk due to the spectral overlap of the fluorophores (*i.e.*, difficulty in selectively exciting donor fluorophores and collecting acceptor emission).[27] Furthermore, the FRET approach requires a high density of fluorophores that can affect/influence polymer conformation as well as complicating the synthesis procedures and interpretation of fluorescence under different conditions (*i.e.*, where the fluorescent properties of one or both fluorophores might differ under a given condition). Therefore, the development of different fluorescence concepts towards high resolution spatially resolved sensing is needed, ideally toward greater dynamic range sensing capabilities and at complex interfaces (*i.e.*, at droplets on a polymer brush).

Herein, we explore a concept of randomly distributed single molecular fluorophores in copolymer brushes, where the concentration of fluorophores is dependent on the polymer brush height, leading to an aggregation induced quenching of the fluorescence. This translates to a concentration based quenching of the fluorescence lifetimes with changing polymer brush height, which can be readily resolved with fluorescence lifetime imaging microscopy (FLIM). This was used to monitor polymer brush conformation both in bulk solvent and at liquid interfaces and to identify solvent swelling of polymer brushes outside of droplets. Our FLIM based method allows for highly sensitive and high resolution sensing of surface polymer brush solvation that is not readily possible by other methods and offers a basis to spatially resolve conformational changes of polymer brushes at complex interfaces.

RESULTS AND DISCUSSION

Polymer Synthesis and Brush Assembly. For the synthesis of fluorophore integrated random copolymers, we synthesized an acrylate monomer composed of Rhodamine B (Rhod B) through conjugation of 2 hydroxylethyl acrylate (HEA) to a Rhod B acyl chloride (Scheme 1). We chose Rhod B as the base fluorophore due to its strong fluorescent properties and ability to be incorporated within dense polymer brushes.[22,26] ^{1}H NMR confirmed the successful modification of

Final edited form was published in "ACS nano". 16 (2), S. 3383–3393. ISSN: 1936-086X.
https://doi.org/10.1021/acsnano.2c00277

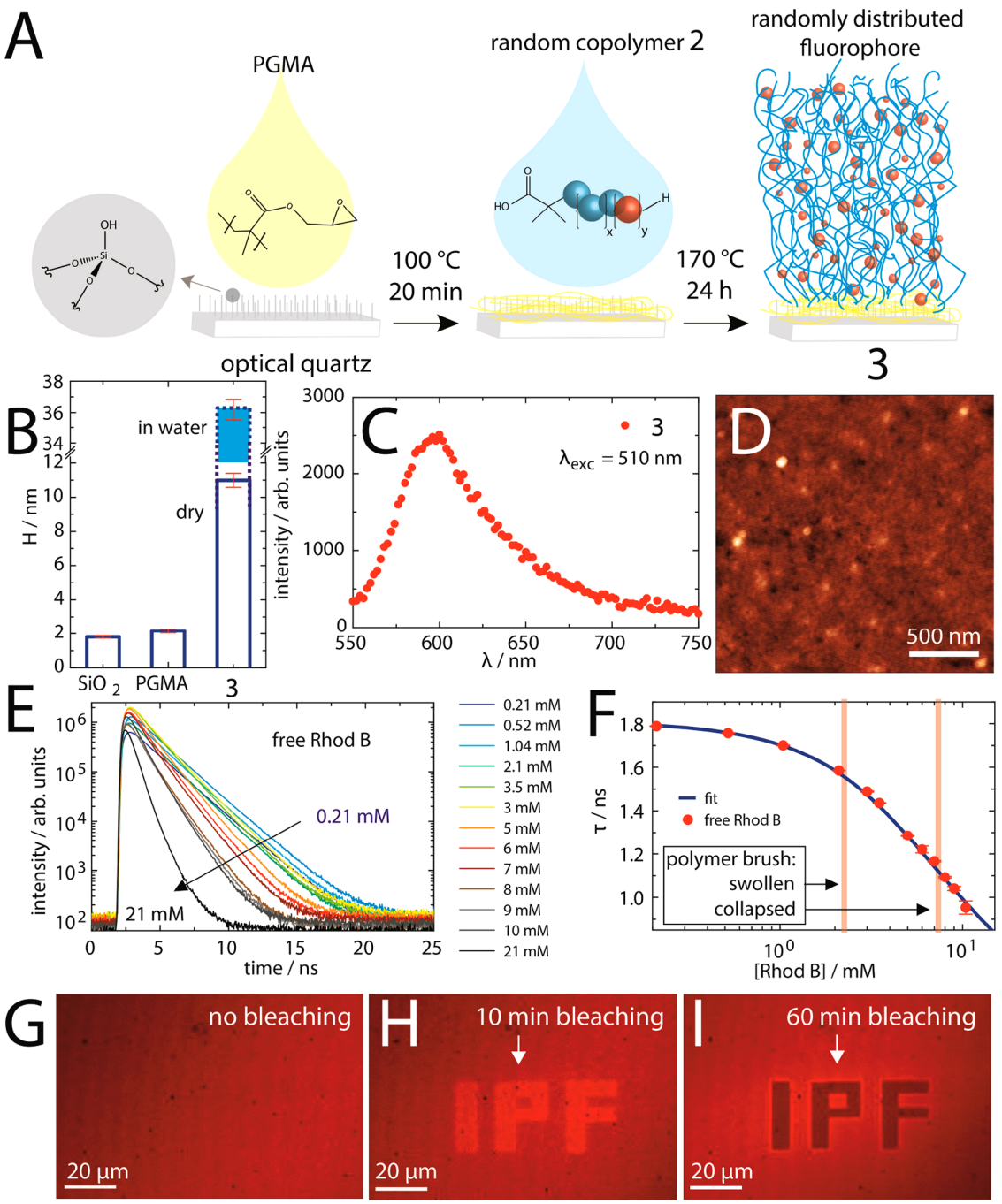

Figure 1. (A) Schematic for the assembly of 2 as polymer brushes on poly(glycidyl methacrylate)(PGMA) coated optical quartz surfaces along with (B) ellipsometry measurements of the thicknesses of each layer and the final product in both wet and dry states with (C) the fluorescence emission spectra from excitation at 510 nm and (D) an AFM topographical image. (E) The intensity decay profiles of standard solutions of Rhod B in Milli Q water along with (F) the intensity weighted fluorescence lifetimes. The vertical red lines indicate the concentration of Rhod B in 3 between the extremes of being solvated and fully collapsed. Confocal laser scanning microscopy (CLSM) was used to measure the surface emission (G) before and after a short period (10 min) (H) and (I) a longer period of photobleaching in a pattern (IPF, Institut für Polymerforschung).

Rhod B (Figure S1A). For the polymer backbone, we chose poly(*N* isopropylacrylamide) (PNIPAM) due to its excep tional responsiveness to solvent stimuli and ability to be assembled into dense polymer brushes.[11,22,26] PNIPAM exhibits co nonsolvency effects, where the chains undergo phase transitions at intermediate mixing ratios of two "good" solvents, such as water/alcohol mixtures,[3] which provides an excellent stimulus to probe conformational effects through subtle changes in aqueous mixture composition.

Reversible addition−fragmentation chain transfer (RAFT) polymerization was performed from a one pot mixture of Rhod B−HEA and NIPAM with azobis(isobutyronitrile) (AIBN) as the radical initiator and 2 (dodecylthiocarbonothioylthio) 2 methylpropionic acid (DDMAT) as the chain transfer agent (CTA). DDMAT was purposefully chosen for the tail carboxylate group for later polymer brush conjugation. The product polymer **1** was pink in appearance (Figure S2) and gave UV−vis spectra showing a clear absorption of Rhod B and

Final edited form was published in "ACS nano". 16 (2), S. 3383–3393. ISSN: 1936-086X.
https://doi.org/10.1021/acsnano.2c00277

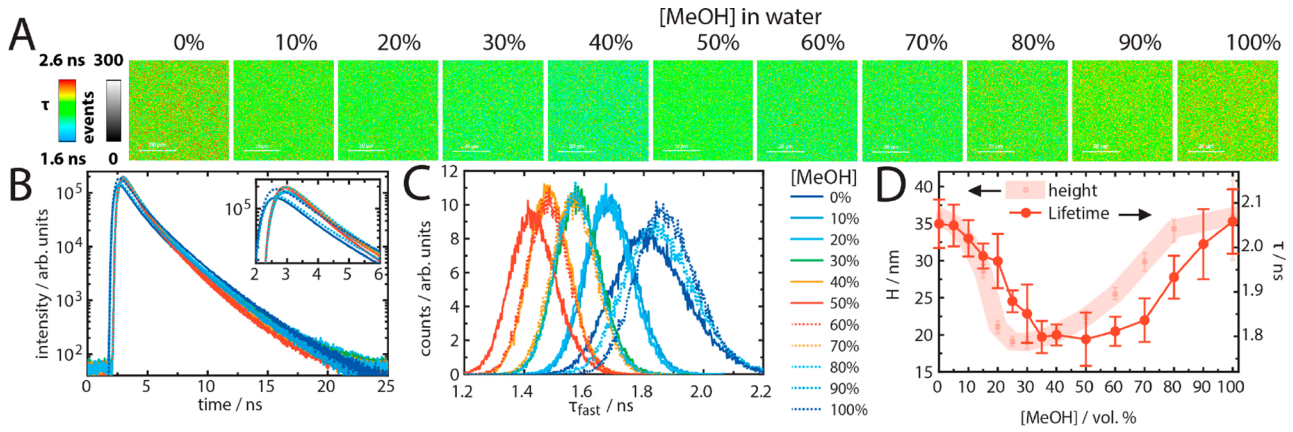

Figure 2. (A) FLIM intensity weighted lifetime images of polymer brush 3 in various MeOH solutions (vol %, scale bar is 30 μm) along with (B) fluorescence lifetime decay curves and (C) fast lifetime histograms for the same mixtures and (D) a direct comparison between the polymer brush height as measured by spectroscopic ellipsometry against the intensity averaged fluorescence lifetime.

of the CTA trithiocarbonate group with a number averaged molecular weight (M_N) of 61.5 kDa ($Đ$ = 1.48) (Figure S3A,B). The CTA group was subsequently removed to yield product **2** by radical induced reduction in the presence of *N* ethylpiperidine hypophosphite (EPHP),[28] which was confirmed by UV−vis (Figure S3A) with M_N remaining the same (61.2 kDa, $Đ$ = 1.48). This second step was performed so as to remove the possibility of additional hydrophobic interactions from the CTA group on the later polymer brush dynamics. A UV−vis standard assay was performed for the Rhod B−HEA monomer in methanol (MeOH) solutions in order to calculate the amount of Rhod B per polymer chain (N_{RhodB}). Through linear regression analysis, it was determined that on average every chain of product **2** contains 0.392 molecules of Rhod B. The starting conditions were 1:1 of Rhod B−HEA to DDMAT, therefore indicating that the Rhod B−HEA monomer was less competitive than NIPAM during the RAFT reaction, though the incorporation is suitable for our purposes.

Polymer brushes were assembled by a macromolecular anchoring approach from a polymer melt. This grafting to method has been shown to consistently yield dense polymer brushes with grafting densities ≥ 0.13 chains/nm^2.[13,22,26] For this approach, the surfaces (either silicon (Si) wafers or optical quartz glass) were thoroughly cleaned and activated by oxygen plasma treatment to expose surface Si−OH groups. To this, a thin layer of poly(glycidyl methacrylate) (PGMA) in chloroform was spin coated (Figure 1A) and allowed to conjugate to the surface Si−OH groups over a short period at elevated temperature. Subsequently, a solution of **2** in tetrahydrofuran (THF) was spin coated on top of the PGMA layer, and the polymer was allowed to conjugate to the PGMA epoxide groups for 24 h at 170 °C. The conjugation of polymer **2** to the PGMA occurred by an esterification of the carboxylate group of the DDMAT CTA to the active epoxide rings of PGMA, leaving the polymer anchored with the reduced R−H chain end away from the surface. The resulting end tethered polymer brush contained randomly distributed Rhod B throughout the structure (product **3**). The dry height of **3** was characterized by single wavelength ellipsometry to be 11 nm ± 0.4 nm (Figure 1B), compared to a 2.1 nm layer of PGMA and a native 1.8 nm Si−OH layer of the substrates. The density of the end grafted chains was determined from $\sigma = (H_d \rho N_A)/M_N$,[29] where H_d is the dry brush thickness, ρ is the bulk density of the polymer composition, which is taken as 1.1 g cm^{-3},[22] and N_A is Avogadro's number. We found that, for **3**, $\sigma \approx 0.124$ chains/nm^2, consistent with previous reports of densely grafted PNIPAM polymer brushes.[13,22] Importantly, the surfaces exhibited strong fluorescence (Figure 1C) and a low root mean square surface roughness of 543 pm (Figure 1D).

The basis of our polymer brush **3** is that the polymer backbone separates Rhod B molecules in space and that, if a stimulus causes the polymer to collapse, the Rhod B concentration increases (*i.e.*, a smaller volume in which the Rhod B is confined). Given the knowledge of σ and N_{RhodB}, we can estimate the concentration of Rhod B as a function of polymer brush height, H, as $C_{RhodB} = N_{RhodB}\sigma/HN_A$. Spectroscopic ellipsometry was used to quantify the "wet" polymer brush height in a good solvent, water, which gave a brush height of ∼36 nm. Therefore, between the extremes of dry (collapsed) and swollen (in water) states, the effective concentration of Rhod B in the volume of polymer brush above the quartz surface is 7.4 and 2.2 mM, respectively. Importantly, previous studies of Rhodamine 6G in methanol have indicated the onset of fluorescence lifetime self quenching from ∼1 mM.[30] We verified the concentration regimes where this self quenching exists for Rhod B by measuring the change in fluorescence lifetimes as a function of concentration in Milli Q water. It was readily seen that the fluorescence intensity decay profiles became shorter as a function of concentration (Figure 1E). Typically, the intensity decay with time, $I(t)$, is fitted by a sum of exponentials such that

$$I(t) = \sum_i A_i e^{-t/\tau_i} \tag{1}$$

where A_i and τ_i are the amplitudes and fluorescence lifetimes for lifetime species *i*. For our analysis, we found that the intensity decays are best fitted by two fractions (*i.e.*, two populations of fluorescence lifetimes), where we use the intensity weighted fluorescence lifetime (*i.e.*, average lifetime) defined as

$$\tau = \frac{\sum_i A_i \tau_i^2}{\sum_i A_i \tau_i} \tag{2}$$

It was found that the average fluorescence lifetime of Rhod B exhibits an onset of significant concentration based quenching from ∼2 mM in Milli Q water (Figure 1F) where the fit

Final edited form was published in "ACS nano". 16 (2), S. 3383–3393. ISSN: 1936-086X.
https://doi.org/10.1021/acsnano.2c00277

demonstrates consistency with the previous studies of Rhodamine 6G (see the Supporting Information). Importantly, the concentration of Rhod B in **3** matches the steep onset of self quenching of Rhod B (marked as red vertical lines in Figure 1F). This implies that the collapsed dry brush exhibits significant self quenching upon excitation. To investigate this, we used confocal laser scanning microscopy (CLSM) in which first a region was scanned for Rhod B fluorescence (Figure 1G) and after a region with a specific pattern ("IPF" = Institut für Polymerforschung) was selected for intense scanning at full laser power for 10 min. It was found that, after 10 min, the patterned region exhibited more intense fluorescence than the surrounding polymer brush, indicating that once some Rhod B was photobleached, the remaining Rhod B could fluoresce stronger due to a lack of self quenching. This was further validated by continuing the photobleaching for a further 60 min, where the resulting area then showed a large loss of fluorescence due to the full photobleaching. Together, this demonstrates that the polymer brush is able to hold Rhod B at a concentration where self quenching effects are strong. Therefore, we looked toward quantifying the polymer brush fluorescence lifetimes *in situ* with stimuli that cause drastic changes in polymer conformation.

Spatially-Resolved Fluorescence. The use of PNIPAM as the polymer backbone means the brushes respond in conformation to alcohol in water mixtures (the co nonsolvency effect). This effect was used as a basis to probe changes in polymer conformation *via* fluorescence lifetime imaging microscopy (FLIM), which allowed for spatial identification of pixel by pixel fluorescence lifetimes of the polymer brush **3**. We performed FLIM measurements of brush samples that were wet by water−MeOH mixtures (Figure 2A), where it was clear that, for intermediate mixing ratios of MeOH in water (*i.e.*, bad solvent), the fluorescence lifetime of the polymer brush decreased. This is consistent with the self quenching due to the Rhod B−Rhod B proximity within the brush. Upon the addition of more "good" solvent (*i.e.*, MeOH), the lifetimes then recovered towards the initial magnitude. This was investigated more closely through the intensity decay profiles (Figure 2B) and the subsequent fast lifetime distributions (Figure 2C), where it was found that the fast lifetime was the lowest for 50% MeOH in water (vol %). For a comparison to polymer conformation, the intensity weighted lifetimes were determined (eq 2) and compared directly to spectroscopic ellipsometry measures of polymer brush height (Figure 2D). It was found that the change in fluorescence lifetime exhibited a similar behavior for solution composition to the change in polymer brush height, albeit with a delay in the minimum and point of recovery from co nonsolvency, which resulted in an offset between the two quantities (Figure S4). For the height, the minimum was found at ∼30% MeOH, while for the fluorescence lifetime, it was at ∼50% MeOH. This likely reflects a mixing dynamic between the polymer chains probed by current spatially resolved fluorescence measurements, which cannot be resolved by spectroscopic ellipsometry, which only resolves the equilibrium brush thickness. Interestingly, the behavior of polymer brush **3** under co nonsolvency matches that of similar pure PNIPAM brushes (*i.e.*, no fluorophore); however, the magnitude of the swelling in the polymer brush height was reduced (∼36 nm compared to ∼57 nm),[11] likely indicating how the incorporation of Rhod B may hinder the swelling of the chains in good solvents. Crucially, Figure 2D verifies that the change in polymer brush height leads to self quenching between the fluorophores and thereby shorter fluorescence lifetimes. This makes the combination of FLIM with the presented polymer brush **3** system a powerful tool for spatially observing polymer conformation.

We point out that the magnitude of the fluorescence quenching in Figure 2D is less than the corresponding quenching of Rhod B solutions in Figure 1F. The swollen brush has an intensity weighted lifetime of ∼2.1 ns, compared to the same concentration of Rhod B at ∼1.6 ns. Furthermore, it is important to consider how differences in solvent/conditions can effect fluorescence lifetime outside of the polymer brush transitions. The fluorescence self quenching of Rhod B has been well studied; there are several mechanisms that affect the fluorescence, including, but not limited to, long range dipole−dipole and collisional energy transfer from monomers to aggregates as well as energy migration between monomers.[31] These different quenching pathways tend to be dependent on solvent due, in part, to differences in solvated distances between fluorescent monomers, dimers, and in some instances, trimers and higher order structures. For example, ethanol has a greater abundance of trimer structures in bulk solution, which contributes to greater quenching.[31] We found that the fluorescence lifetimes of bulk Rhod B in water and in pure methanol are different by about ∼0.5 ns (Table S1), yet the polymer brushes have the same fluorescence lifetime in pure water and pure methanol, therefore pointing toward a difference in the quenching mechanisms between bulk Rhod B and the polymer brush **3**. Furthermore, we investigated the fluorescence lifetime of free Rhod B in water and MeOH solutions of different NIPAM concentrations as a means to rule out solvatochromic effects. It was found that the fluorescence lifetime of Rhod B increases as a function of NIPAM concentration and, at 2 M NIPAM (toward the upper solubility of NIPAM in water), the fluorescence lifetime of Rhod B in water and MeOH is effectively the same (Table S2). The concentration of polymerized NIPAM in the polymer brush **3** is ∼3 M. Together, this indicates that the NIPAM monomer units are able to prevent aggregation induced changes in the fluorescence lifetime of Rhod B in both water and MeOH systems, which rules out solvatochromic differences in the solvent systems in Figure 2 and, therefore, supports our hypothesis of concentration induced quenching of Rhod B's fluorescence as a function of polymer brush conformation in product **3**. We point out that the structure of the free NIPAM monomer compared to the polymerized monomer is significantly different, but it does provide a good probe of concentration based dependencies on the Rhod B fluorescence lifetime.

It is anticipated that the results for the NIPAM systems will have similar, but effectively different, qualities to the polymer brushes. For our polymer brush structures, the Rhod B molecules are covalently tethered and surrounded by PNIPAM chains. This leads to a significantly different solvation environment than both the bulk Rhod B and Rhod B/NIPAM solutions and, likely, a different ability of the Rhod B molecules to exhibit specific orientations with respect to one another that may lead to dimer and trimer induced quenching as well as collisional energy transfer processes. It has been suggested by Setiawan *et al.*[32] that preventing certain arrangements of transition dipole moments between Rhod B molecules, such as by incorporating into a matrix or anchoring to a surface, can lead to greater fluorescence quantum yield. This is the basis of our hypothesis for the differences in

Final edited form was published in "ACS nano". 16 (2), S. 3383–3393. ISSN: 1936-086X.
https://doi.org/10.1021/acsnano.2c00277

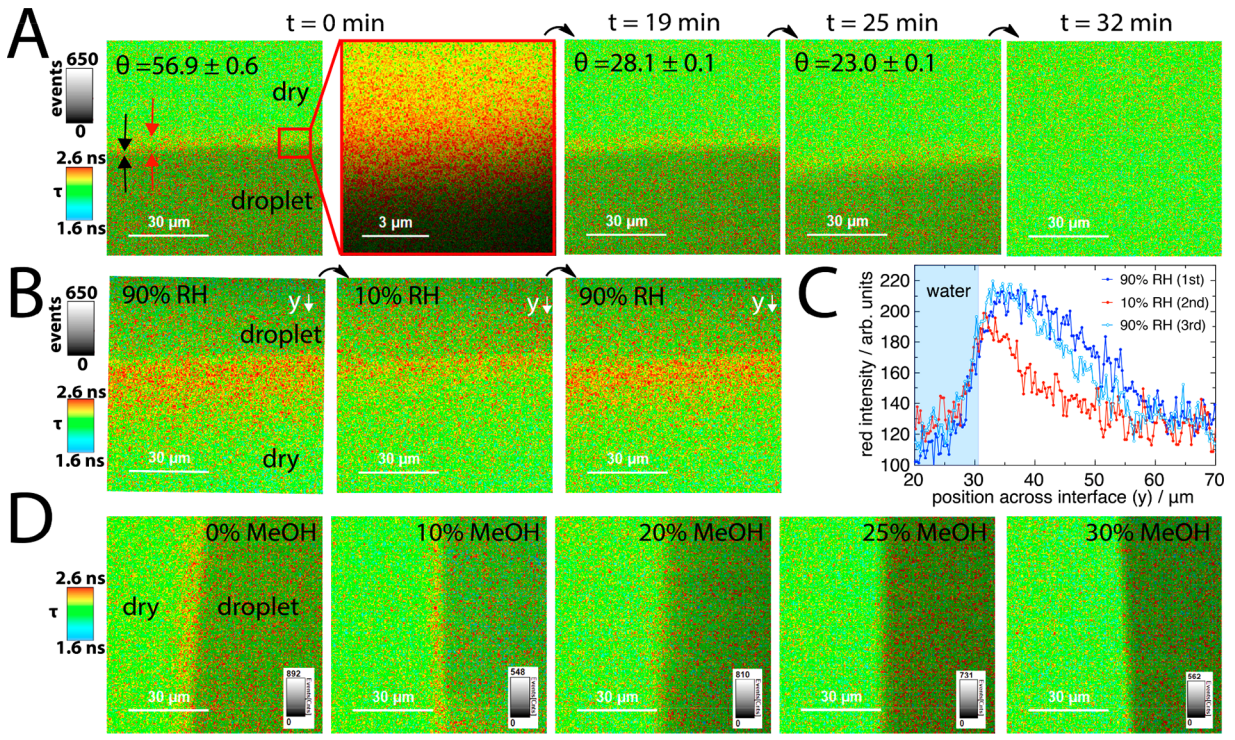

Figure 3. (A) Sequential FLIM images of the air−liquid interface of a 6 μL water droplet on the polymer brush surface 3 as a function of time at 22 °C and 49% relative humidity (RH), where black pinching arrows indicate the direct interface as seen by intensity and the red arrows indicate the region of perturbed fluorescence lifetimes outside of the direct droplet. (B) FLIM images of a 6 μL water droplet as a function of RH and (C) the corresponding red intensity line profile across the interface (ImageJ RGB profile). (D) FLIM images of droplets of different water−MeOH mixtures (6 μL, 22 °C, and 49% RH). All FLIM images are intensity weighted and gated by 1.6−2.6 ns and show events of 0−650 counts, unless otherwise shown in the graphic.

lifetimes between tethered Rhod B in the polymer brush and free Rhod B solutions and also for the similarities in fluorescence lifetime between pure water and pure methanol.

With the fluorescence lifetime dependence of polymer brush **3** verified, the use of FLIM was then explored to investigate polymer conformation effects around complex interfaces, such as the air−water−solid interface of a water droplet (Figure 3A). It was found that the fluorescence lifetime of the water phase and the dry phase was relatively similar, which is likely due to a complex interplay of AIE effects that affect the fluorescent lifetimes. However, at the interface, just outside of the droplet edge, a clear region of longer lifetime species was observed. This region spanned ∼5 μm from the direct droplet edge at 49% relative humidity (RH) and 22 °C. The edge of the droplet was judged from the fluorescence intensity (*i.e.*, events) where the water solvated area was less fluorescent than the dry area, likely due to AIE effects and scattering and absorption by the liquid, which has been observed previously.[26] Interestingly, as this region was observed with time, it remained relatively constant in width and lifetime as the water droplet evaporated off and the contact angle reduced (∼57° to ∼28°) before the droplet receded away (imaged at 25 min and 23°, as the droplet was receding). After the droplet had receded, there was also no clear "scarring" or memory of where the contact line was. Due to the length scales involved (*i.e.*, ∼5 μm perturbation of lifetime from a ∼36 nm polymer brush on a rigid substrate), it is unlikely that this change in lifetime is due to contact line forces deforming the interface. We therefore investigated if the perturbation was due to solvent swelling of the polymer brush outside of the droplet by controlling the RH of the system above the surface (Figure S5).

It was found that when the system was held at 90% RH, at which the droplet can only slowly evaporate, and after allowing equilibration over 7 min, the region of perturbed lifetimes became significantly larger reaching 15−20 μm from the droplet's edge (Figure 3B). Furthermore, when the system was subsequently reverted to 10% RH and allowed to equilibrate (*i.e.*, evaporation can occur readily), this region reduced back toward 5 μm. Then, upon cycling back to 90% RH, this region again expanded toward 15−20 μm from the droplet's edge. This is consistent with the perturbed region reflecting the swelling of the polymer brush outside of the water droplet. We hypothesize that the brush swelling is in local equilibrium with the vapor concentration in the atmosphere directly above the brush. The local vapor pressure in the atmosphere is influenced by the evaporation from the droplet and the relative humidity far away from the droplet. Close to the droplet, the vapor pressure is increased and, therefore, the swelling of the brush occurred. Information on the swelling of polymer brushes at such an interface at this resolution is not available from other methods to the best of our knowledge. We further tested this concept by imaging the edge of co nonsolvency droplets (Figure 3D), where in the co nonsolvency regimes no significant swelling should occur (*i.e.*, the polymer is collapsed), and we found that this edge region was present for 0−10% MeOH but was not present to a significant degree for 20−30% MeOH (Figure S6), again consistent with our method revealing a swelling of the polymer brush.

To better understand what occurs to the polymer brush as the solvent swells the chains outside of the droplet and why

Final edited form was published in "ACS nano". 16 (2), S. 3383–3393. ISSN: 1936-086X.
https://doi.org/10.1021/acsnano.2c00277

this appeared to be different from the bulk area underneath the droplet (Figure 3A), we performed coarse grained molecular dynamics (MD) simulations of model copolymers that have pseudo fluorophores randomly positioned in each chain. A hydrophobic like potential was given to the fluorophores in order to reflect the hydrophobic nature of Rhod B, which has a log partition coefficient of ∼5.5 for octanol/water.[33] The brushes were sequentially solvated by different amounts of water that were added directly onto the surface (Figure 4). It

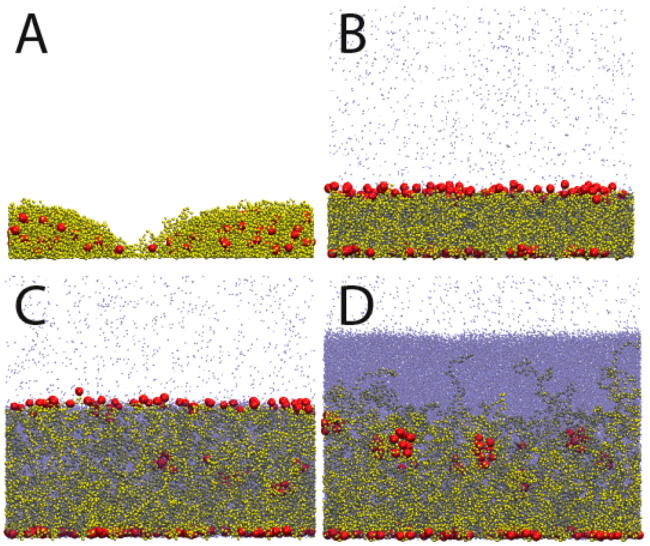

Figure 4. Simulation snapshots of model polymer brushes (rendered yellow) with chromophores randomly distributed on the chains (rendered red) being sequentially swelled by solvent (shaded blue rendering) corresponding to dry (A), half swelled (B), fully swelled (C) and fully submerged (D) states. The number of water molecules in the simulations was 28 444, 71 111, and 113 778 molecules for (B), (C), and (D), respectively.

was found that, as water began to swell the dry surface (Figure 4A,B), the fluorophores separated to each of the outside edges (*i.e.*, to the anchoring surface and to the vapor phase). Then, as more solvent was added, the fluorophores clearly extended away from the solvated polymer, creating a "pulling" effect on the polymer chains (Figure 4C). As the solvent then fully submerged the polymer brush (Figure 4D), the fluorophores no longer stretched toward the vapor phase and instead started to cluster closer to the surface. In this situation, the polymer chains extended more entropically into the water phase. This showed how the fluorophores can affect the conformation of the brush with different surface and vapor phase affinities than the polymer. However, we point out that the relationship between fluorophore proximity (concentration/aggregation) and the fluorescence lifetime is not clear as the fluorescence quenching is the result, in part, of specific aggregate states (dimers, trimers, *etc.*)[31] and orientations,[32] which cannot be captured by MD simulations of spherical Lennard Jones beads. Furthermore, this highlights where the integrated fluorophores can potentially lead to transitions in polymer brush conformation that are not anticipated from the PNIPAM alone though, as seen in Figure 4C,D, this is small in comparison to the transitions from collapsed to swollen states. For example, the ensemble average height for the fully submerged brush is ∼94% of that of the fully swollen brush (Figure S7).

It is not readily obvious if the swelling of the brush is due to solvent (water) diffusion from within the droplet or from vapor condensing onto the polymer brush just outside of the droplet although it is likely an interplay of both processes. Recently, Ritsema van Eck *et al.*[34] reported on MD simulations of polymer brushes at equilibrium with solvent vapor, where it was found that solvent uptake into the brush resulted in a strong swelling of the brush. On the other hand, when solvent adsorption was prevented (*i.e.*, stronger polymer−polymer affinity than polymer−solvent), the interior of the brush contained very little to no solvent. A translational entropy led to limited solvent penetration into the brush, but chain stretching was precluded by the associated entropic penalty. This is in excellent conceptual agreement with our current results for the swelling outside of both the water and co nonsolvency droplets.

Our presented FLIM sensitive polymer brush surfaces offer an intriguing platform to investigate the surface wetting at immiscible liquid−liquid interfaces. Recently, we reported on FRET integrated polymer brush surfaces that revealed less FRET at a hexane−water interface, consistent with an extended polymer brush in this region.[26] Here, we investigated this same interface as well as the toluene−water interface with FLIM of **3**. This was done by first placing a droplet of water on the polymer brush surface and then adding a bath of hexane or toluene to the surrounding surface in such a volume that the entire surface was well covered with organic solvent (Figure S8). Similar to Figure 3A,B, it was found that, at just outside of the water phase, there was an increase in the fluorescence lifetime over a region spanning ∼30−40 μm before the lifetime drastically reduced deeper in the oil phase (Figure 5). This was

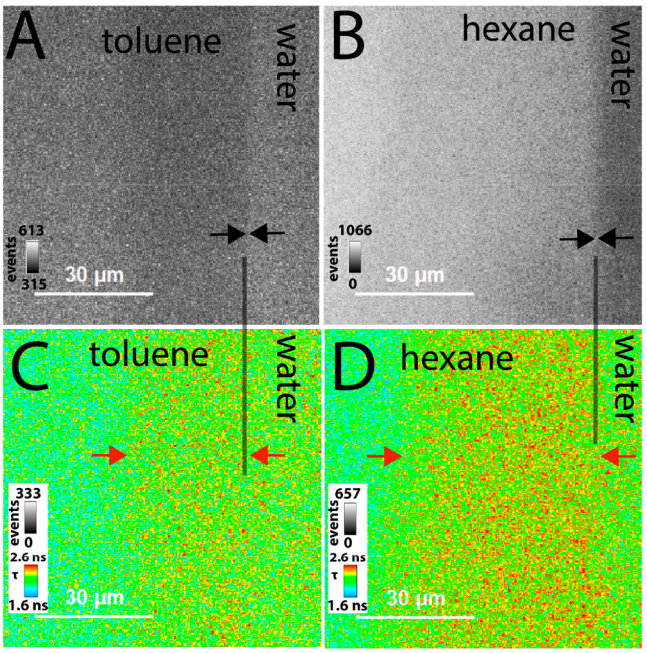

Figure 5. Bright field images of the toluene−water (A) and hexane−water (B) interfaces and the corresponding FLIM images (C) and (D), respectively). The black arrows (to guide the eye) indicate the direct interface, as judged from fluorescence intensity images, whereas the red arrows indicate the perturbed polymer brush directly outside of the visible contact line. Note the "bulk" fluorescence lifetime of the organic phase is situated on the far left of the images. Measurements performed at 21.9 °C and 49.3% RH.

Final edited form was published in "ACS nano". 16 (2), S. 3383–3393. ISSN: 1936-086X.
https://doi.org/10.1021/acsnano.2c00277

more dramatic for the hexane−water interface than for the toluene−water interface, which we concluded reflects different mixing dynamics/thermodynamics at the interface and with the polymer brush surface itself. The fluorescence lifetimes underneath the bulk toluene and hexane phases were equivalent, demonstrating that the difference is only due to an effect at the interface itself, where the lifetimes in these bulk phases were reduced in comparison to that in the water phase. Importantly, this result is consistent with the previous studies of the same interface (hexane−water)[26] and is strongly linked to the mechanism revealed in Figure 4 with Rhod B providing a hydrophobic "pull" as water solvates the polymer, thereby revealing a strong swelling of the polymer brush at these complex interfaces with the Rhod B modified units extended toward the oil phase.

Lastly, our single fluorophore integrated polymer brushes offer several advantages over the previously reported FRET based systems.[26] Namely, the sensitivity (in terms of pixel by pixel acquisition) is enhanced for spatially resolved sensing with 5× less fluorophores required and of only a single fluorophore type (Rhod B in this case). This approach therefore overcomes the limitations that are inherent to the FRET approach, and not least of which, it greatly simplifies the synthetic procedures required to generate mechanofluorescent polymer brushes. With the presented system, it becomes feasible to make surface based senses to investigate complex surface adhesion phenomena (*e.g.*, cell adhesion) and localized changes in polymer brush conformation from spatially controlled stimuli (*e.g.*, region specific changes in pH, temperature, solvent, *etc.*).

CONCLUSIONS

When a polymer brush undergoes a phase transition during collapse, the effective volume held by the polymer becomes smaller, and therefore, the polymer concentration becomes greater. We have developed single fluorophore integrated polymer brush surfaces that leverage this conformation controlled concentration modulation as a basis for sensing conformation through self quenching effects of the fluorophores. It was found that the concentration regime, whereby Rhod B exhibits significant self quenching effects, can be achieved through the grafting to of random copolymers of NIPAM and Rhod B to macromolecular PGMA anchoring layers on optical quartz surfaces. The conformation controlled fluorescence lifetimes were verified by comparisons between fluorescence lifetime imaging microscopy and spectroscopic ellipsometry measures of brush thickness. These surfaces were used as a basis for sensing polymer conformation effects around complex interfaces, including the air−water−solid interface of a dispersed water droplet, and across the interfacial regions of immiscible liquids that solvate the surface polymer brush. This revealed information on the swelling of polymer brushes outside of direct droplets and highlighted where good solvents can swell the brush when there is bad solvent above the brush. Our surfaces offer great potential for different surface based sensing capabilities to be realized, primarily due to their simplicity, and we expect they will hold high utility in complex mechanosensing studies with high spatial resolution.

EXPERIMENTAL SECTION

Materials. All chemicals were of analytical grade and used as received without further purification with the exception of 2 hydroxyethlacrylate (HEA) and *N* isopropylacrylamide (NIPAM), which were purified by passing through an aluminum oxide column prior to reaction and by recrystallization from hexane (2×), respectively, to remove inhibitors. High purity water (Milli Q water) with a resistivity of >18.2 MΩ cm was obtained from an inline Millipore RiOs/Origin water purification system (Millipore Corporation, Massachusetts, USA). Polished single crystal (100) silicon wafers were obtained from Silicon Materials, Kaufering, Germany, with a native SiO_2 layer thickness of ∼1.8 nm. Optical fused quartz square coverslips (22 × 22 × 0.2 mm) were obtained from Micro to Nano (Haarlem, The Netherlands). PGMA (M_N = 15 000 g mol^{-1}, $Đ$ = 1.6) was obtained from Polymer Source Inc. (Montreal, Canada). Acetonitrile (ACN), ethanolamine, 4 chloro 7 nitrobenzo furazan (NBD Cl), acryloyl chloride, thionyl chloride, dichloroethane (DCE), Rhodamine B (Rhod B), HEA, dichloromethane (DCM), NIPAM, azobisisobutynitrile (AIBN), 2 (dodecylthiocarbonothioylthio) 2 methylpropionic acid (DDMAT), 1 ethylpiperidine hypophosphite (EPHP, 95%), 1,4 dioxane (anhydrous), diethyl ether, toluene, chloroform, hexane, 1,4 dioxane (anhydrous), ethanol, and methanol were obtained from Sigma Aldrich. Tetrahydrofuran (THF) was obtained from Acros Organics. Chloroform was obtained from Fisher Chemicals. $CDCl_3$ was obtained from Eurisotop (Saint Aubin, France). Dialysis membrane was obtained from Repligen (Breda, The Netherlands).

Synthesis of Rhod B−HEA. Rhod B (2.1 mmol, 1 g) was dissolved in DCE (18 mL) to which thionyl chloride (12.7 mmol, 921 μL) was added dropwise at 23 °C with stirring. After 30 min, the system was then refluxed for 12 h. The solvent was subsequently removed under reduced pressure, and the crude product was redissolved in DCM (15 mL) to which HEA (9.6 mmol, 1.04 mL) was added dropwise; the system was left to stir overnight at 23 °C. The solvent was subsequently removed under reduced pressure, and the crude product was purified by column chromatography (DCM/MeOH, 30:1) to yield a red sticky solid (581 mg, 51.1% yield). ^{1}H NMR (400 MHz, $CDCl_3$, 25 °C, δ): 8.34 (d, 1H), 7.90 (t, 1H), 7.79 (d, 1H), 7.48 (d, 1H), 7.39 (d, 1H), 7.17 (d, 1H), 6.41 (d, 1H), 6.10 (m, 1H), 5.87 (d, 1H), 5.31 (s, 1H), 4.31 (m, 5H), 3.97 (s, 1H), 3.89 (m, 6H), 3.73 (q, 1H), 1.42 (t, 12 H), 1.27 (m, 4H).

Synthesis of RAFT Polymer 1. NIPAM (30.4 mmol, 3.53 g), AIBN (0.0152 mmol, 2.5 mg), Rhod B−HEA (0.154 mmol, 42.9 mg), and DDMAT (0.154 mmol, 56 mg) were added to a 15 mL Schlenk tube equipped with a stirrer bar to which anhydrous 1,4 dioxane (6 mL) was added. The mixture was then degassed by bubbling argon for 1.5 h. Polymerization was initiated by heating the mixture to 70 °C with rigorous stirring. The flask was protected from light and allowed to react overnight. After 16 h, the mixture was then exposed to air, and the solvent was removed under reduced pressure. The crude polymer was then redissolved in minimal THF before being precipitated into cold diethyl ether (2 × 250 mL) and dried overnight in a vacuum oven at 40 °C. The product was isolated as a bright red powder (1.9 g).

CTA Group Removal. The RAFT polymer **1** (1 g, 0.0163 mmol CTA) was dissolved in ACN (20 mL) to which EPHP (0.24 g, 1.34 mmol) and AIBN (4 mg, 0.024 mmol) were added, and the system was degassed by bubbling argon for 1 h. Subsequently, the system was refluxed at 100 °C for 2.5 h. The solvent was then extracted under reduced pressure; the crude product was dispersed in Milli Q water and then dialyzed against Milli Q for 3 days (8 L, 5 kDa cutoff) before isolating the pure product **2** by freeze drying (0.83 g as a pink fluffy powder).

Formation of Polymer Brushes. Silicon wafers (20 × 13 mm) or fused quartz coverslips (22 × 22 × 0.2 mm) were treated with EtOH in an ultrasonic bath for 20 min at 37 °C and then dried under nitrogen. The cleaned substrates were then activated in an oxygen plasma for 1 min (Harrick, Plasma Cleaner PDC 002 with Plasma Flo PDC FMG). In order to obtain an anchoring layer for the subsequent grafting to process of **2**, a filtered solution of PGMA (80 μL for silicon wafer or 160 μL for quartz of a 0.2 mg mL^{-1} solution in chloroform) was spin coated (Spin150 spin coater, Polos, v = 2000 r min^{-1}, a = 1000 r (min s)$^{-1}$, t = 10 s) onto the activated substrates. The PGMA anchoring layer was subsequently annealed at 100 °C in a vacuum

Final edited form was published in "ACS nano". 16 (2), S. 3383–3393. ISSN: 1936-086X.
https://doi.org/10.1021/acsnano.2c00277

oven for 20 min to react the silanol groups of the substrate with a fraction of the epoxy group of PGMA. The remaining epoxy groups were then used for the subsequent grafting to process, whereby the carboxylate end groups of polymer **2** can esterify on the epoxy rings of PGMA. A filtered solution of **2** (120 μL (silicon wafer) or 240 μL (quartz) of a 11 mg mL^{-1} solution) was subsequently spin coated on the substrates (Spin150 spin coater, Polos, v = 2000 r min^{-1}, a = 1000 r (min s)$^{-1}$, t = 10 s), followed by annealing at 170 °C in a vacuum oven for 24 h. To remove noncovalently bound polymer, the resulting substrates where first immersed in Milli Q water, then extracted in Milli Q water overnight, rinsed with EtOH, and dried under a stream of nitrogen.

Fluorescence and UV−Vis measurements. All measurements were performed with a multimode microplate reader (Tecan Spark 10M, Switzerland). The UV−vis analysis of the free polymer **1** and **2** was performed at a concentration of 1 mg mL^{-1} in methanol. Fluorescence spectra of the product **3** were taken in Milli Q water (λ_{exc} = 510 nm, dλ = 2 nm, 530−700 nm) while the temperature was maintained at 24 °C.

GPC Measurements. The measurements were performed on a SECurtity2 GPC system equipped with a SECurity2 isocratic pump, SECurity2 2 channel inline degasser, one SECurity2 autosampler, one SECurity2 column thermostat TCC6500, equipped with one GRAM precolumn, one GRAM 3000 10 μL, 300 × 8 mm column, and one GRAM 30 10 μL, 300 × 8 mm analytical column, one SECurity2 variable UV−vis detector, one SECurity2 differential RI detector, a SECurity GPC viscosity detector DVD1260, and a DAWN DSP Laser Photometer MALS detector by Wyatt Technology. The oven temperature of the system was set to 50 °C, and the flow was adjusted to 1.0 mL min^{-1}. Dimethylacetamide (DMAc) with 5 g/L LiBr and 1 vol % water was used as the eluent. UV−vis detection was performed at l = 450 nm. The system was calibrated with PMMA standards in a range of 602−2 200 000 g/mol (conventional calibration). All the standards were purchased from Polymer Standard Solutions and used as received. For measurement, the samples were dissolved in the eluent (2−4 mg mL^{-1}), filtered through a 0.2 μm PTFE syringe filter, and afterward injected to the instrument. The molar masses were determined by the signal from RI detection.

Confocal Laser Scanning Microscopy (CLSM). For spatially resolved fluorescence studies of photobleached regions (Figure 1G−I), a combined setup of an Axio Observer Z.1 inverted microscope with an LSM710 confocal laser scanning module (Carl Zeiss Microscopy, Germany) was used with a single 20× objective. The Rhod B was excited with a helium−neon laser (543 nm). The pinhole was set to 1 AU.

Atomic Force Microscopy (AFM). In air tapping mode AFM was performed with a Nanoscope Dimension D3100 V (Veeco Instruments, U.S.A.) with software analysis by NanoScope Analysis 1.7 and with a tapping mode probe (500 kHz, k = 3−4 N m^{-1}, supplied by Budget Sensors Innovative Solutions, Bulgaria Ltd.).

NMR Spectroscopy. The ^{1}H (500.13 MHz) NMR spectra were recorded using an AVANCE III 500 Spectrometer (Bruker, Germany) and $CDCl_3$ at 30 °C.

Spectroscopy Ellipsometry. The measurement and modeling procedures were as reported previously.[35] In brief, a spectroscopic ellipsometer (alpha SE, Woollam Co., Inc., Lincoln, NE, USA) equipped with a rotating compensator was used to measure the relative phase shift (Δ) and the relative amplitude ratio (tan Ψ) of the polymer brush films in the dry state as well as *in situ* in freshly prepared water−methanol mixtures within batch cuvettes (TSL Spectrosil, Hellma, Muellheim, Germany) at a constant temperature of 24 ± 0.1 °C. All measurements were performed between 400 and 800 nm at an angle of incidence (Φ_o) of 70°. To evaluate the index of refraction and thickness of the brush films, a multilayer box model constructed of silicon, silicon dioxide, PGMA, and PNIPAM was assumed. The refractive indices of the liquids was measured using a digital multiple wavelength refractometer (DSR lambda, Schmidt + Haensch, Berlin, Germany). All data was acquired and analyzed using the Complete EASE software package (version 4.46).

Contact Angle. Contact angles of freshly purified water (conductivity of 0.055 μS/cm) from the MicroPure UV/UF device (Thermo Electron LED GmbH) were measured with OCA35XL from Data Physics. Recorded contact angles were analyzed with the SCA20 program from Data Physics. The measurements were performed in a humidity (48 ± 2%) and temperature (23.0 ± 0.5%) controlled lab. Note that contact angle measurements were performed separately from the FLIM measurements.

Molecular Dynamics Simulations. We apply a coarse grained model of the polymers consisting of freely jointed spherical beads that are connected by finite extensible nonlinear elastic (FENE) bonds ("Kremer Grest model").[36] Pair potentials are Lennard Jones (LJ) potentials of the form

$$V_{LJ}(r) = 4\epsilon\left[\left(\frac{d}{r}\right)^{12} - \left(\frac{d}{r}\right)^{6} - \left(\frac{d}{r_c}\right)^{12} + \left(\frac{d}{r_c}\right)^{6}\right]$$

in which ε defines the interaction strength (in units of k_BT, where k_B is Boltzmann's constant and T is the absolute temperature), d is the bead diameter (or in the case of two beads of different diameters, their average value), and r_c is the cutoff distance. A polymer is a bead−spring chain consisting of a backbone of N = 120 beads of diameter d = 1 (defining the length unit). The fluorophores are modeled as side groups of diameter d_c = 2, attached to backbone monomers at random positions (two fluorophores on each chain). To create a brush, 100 chains are end grafted onto an impenetrable substrate in a Cartesian 10 × 10 pattern at a grafting density (σ) of 0.025 (chains per unit area). The area is given in terms of the bead diameter of the monomer units. Water molecules are coarse grained single beads with d = 1. Pair interactions are as follows: ε(monomer−monomer) = 0.6, ε(fluorophore−fluorophore) = 0.6, ε(monomer−fluorophore) = 1.0, ε(water−water) = 1.4, ε(water−monomer) = 1.2, and ε(water−fluorophore) = 1.0. The cutoff length of the LJ potential is $r_c = 2.5d$ with exception of the water−fluorophore interaction, where the potential is truncated at its minimum to eliminate all attractive contributions. With that interaction being fully repulsive, the fluorophores become hydrophobic. The simulation box is periodic in both lateral directions to mimic an infinitely large brush but bounded with LJ walls at the substrate and the upper boundary to prevent particles from escaping the box, which has a height of 70 units.

The simulations are carried out with the open source LAMMPS simulation package.[37] The equation of motion of each bead is the Langevin equation

$$m\frac{d^2r}{dt^2} = -\frac{m dr}{\tau dt} - \frac{\partial V}{\partial r} + F$$

with the mass, m, being 8 for fluorophores and 1 for monomers and cosolvent. The momentum relaxation time, τ, was 4 for fluorophores and 1 for monomers and cosolvent. V is the total potential, and F is the white noise fluctuation force. Each bead is further exposed to a vertical acceleration (a) of 0.003, pointing downward toward the substrate ("gravity"), which is introduced to generate a horizontal phase boundary between liquid water and the vapor. The temperature (T*) was chosen to be 1, and the time step is dt = 0.0025 LJ times. Initially, all chains are random walks in the positive half space above the substrate, and water beads are randomly distributed throughout the simulation box. In a short prerun of 100 000 steps, overlaps among the beads are removed with the help of a gradually increasing repulsive soft potential. It follows a relaxation of 50 million simulation steps to bring the system into equilibrium.

Fluorescence Lifetime Imaging Microscopy (FLIM). Fluorescence lifetime images and time correlated single photon counting (TCSPC) data were measured with an inverted confocal scanning microscope (MT200, PicoQuant) incorporating a 100× air objective (UPFLN, NA 0.9, Olympus, Japan). Diode lasers with a 510 nm central wavelength (LDH 510) and a 13.33 MHz repetition rate were used for excitation. The signal was guided through a long pass filter with a cutoff below 519 nm (FF01 510/LP, Semrock) and detected

Final edited form was published in "ACS nano". 16 (2), S. 3383–3393. ISSN: 1936-086X.
https://doi.org/10.1021/acsnano.2c00277

with a SPCM AQRH single photon counting module (Excelitas). The images based on intensity weighted lifetimes were fitted for fluorescence decays between 4.5 and 25 ns with $n = 2$ lifetimes. The instrument count rates were kept below 1/10th of the laser repetition rate, where a standard intensity sum count rate of 1.5×10^7 events was used. A minimum of 3 separate polymer brush surfaces were used for every study. All measurements were performed at 21.9 °C and 48.9% RH unless otherwise stated. The lifetime is evaluated as the intensity weighted lifetime (eq 2), unless otherwise stated, for the best comparisons between samples. In Figure 2A,C, specifically, we report the fast fluorescence lifetime, which uses the average TCSPC channel to generate a histogram of the average photon delay times. The fast lifetime is obtained as the value minus the first moment of the instrument response function. Because no fitting is involved, this calculation is very fast. However, the drawback is that no further information beyond the fast lifetime can be extracted; hence, for all subsequent analyses, we use the intensity weighted lifetimes. For humidity control, a stream of nitrogen was split and controlled by two flow controllers from ANALYT MTC Meßtechnik GmbH (Müllheim Germany). One stream was saturated with water by guiding it through gas wash bottles (DURAN Group GmbH in Wertheim Germany). When the flow rates of the two streams are varied, the relative humidity of the united stream can be controlled.

For the organic solvent–water interface measurements, a small droplet of water (6 μL) was first added onto the surface, followed by a bath of either hexane or toluene added to the remaining surface. The organic solvent was added in such a volume that the entire surface was covered in solvent. In this system, the water droplet is pinned by the brush, and FLIM measurements were performed on the interface with the organic solvent bath topped off if needed.

ASSOCIATED CONTENT

Supporting Information

The Supporting Information is available free of charge at https://pubs.acs.org/doi/10.1021/acsnano.2c00277.

Experimental and simulation details including ^{1}H NMR spectroscopy, properties of product polymers, concen tration of fluorophores per unit volume, details on the fluorescence lifetime self quenching fits, fluorescence lifetime data of Rhod B in water–methanol mixtures (with and without NIPAM), details on the humidity controlled FLIM, FLIM profiles across co nonsolvency droplet interfaces, brush heights from MD simulations, and details on the solvent–water interfaces (PDF)

AUTHOR INFORMATION

Corresponding Authors

Quinn A. Besford – *Leibniz Institut für Polymerforschung e.V., 01069 Dresden, Germany;* orcid.org/0000 0002 1779 9176; Email: besford@ipfdd.de

Andreas Fery – *Leibniz Institut für Polymerforschung e.V., 01069 Dresden, Germany; Technische Universität Dresden, 01062 Dresden, Germany;* orcid.org/0000 0001 6692 3762; Email: fery@ipfdd.de

Authors

Holger Merlitz – *Leibniz Institut für Polymerforschung e.V., 01069 Dresden, Germany*

Simon Schubotz – *Leibniz Institut für Polymerforschung e.V., 01069 Dresden, Germany*

Huaisong Yong – *Leibniz Institut für Polymerforschung e.V., 01069 Dresden, Germany*

Soosang Chae – *Leibniz Institut für Polymerforschung e.V., 01069 Dresden, Germany*

Max J. Schnepf – *Leibniz Institut für Polymerforschung e.V., 01069 Dresden, Germany*

Alessia C. G. Weiss – *Leibniz Institut für Polymerforschung e.V., 01069 Dresden, Germany*

Günter K. Auernhammer – *Leibniz Institut für Polymerforschung e.V., 01069 Dresden, Germany;* orcid.org/0000 0003 1515 0143

Jens Uwe Sommer – *Leibniz Institut für Polymerforschung e.V., 01069 Dresden, Germany; Institute for Theoretical Physics, Technische Universität Dresden, 01069 Dresden, Germany*

Petra Uhlmann – *Leibniz Institut für Polymerforschung e.V., 01069 Dresden, Germany;* orcid.org/0000 0001 9298 4083

Complete contact information is available at: https://pubs.acs.org/10.1021/acsnano.2c00277

Author Contributions

The project was conceptualized by Q.A.B. The manuscript was written through contributions of all authors. All authors have given approval to the final version of the manuscript.

Notes

The authors declare no competing financial interest.

ACKNOWLEDGMENTS

This research was funded by the Alexander von Humboldt foundation (Q.A.B.). The Deutsche Forschungsgemeinschaft (DFG) is gratefully acknowledged for funding through project 422852551 (AU321/10 1, FE600/32 1, UH121/3 1) within the priority program 2171, grant SO 277/12 1, and project ID 265191195–SFB1194. We gratefully acknowledge Laura Fietzke and Rainer Jordan from the Technische Universität Dresden for assistance with GPC, Hannes Kettner, Eva Bittrich, and Peyman Rostani, all from IPF Dresden, for assistance with AFM, ellipsometry, and infrared imaging, respectively, and Willem van den Heuvel, Alexander Münch, Shuaijun Pan, Andrew Christofferson, and Aaron Elbourne for fruitful discussions.

REFERENCES

(1) Heggestad, J. T.; Fontes, C. M.; Joh, D. Y.; Hucknall, A. M.; Chilkoti, A. In Pursuit of Zero 2.0: Recent Developments in Nonfouling Polymer Brushes for Immunoassays. *Adv. Mater.* **2020**, *32*, No. 1903285.

(2) Hou, J.; Chen, R.; Liu, J.; Wang, H.; Shi, Q.; Xin, Z.; Wong, S. C.; Yin, J. Multiple Microarrays of Non Adherent Cells on a Single 3D Stimuli Responsive Binary Polymer Brush Pattern. *J. Mater. Chem. B* **2018**, *6*, 4792–4798.

(3) Yu, Y.; Cirelli, M.; Kieviet, B. D.; Kooij, E. S.; Vancso, G. J.; de Beer, S. Tunable Friction by Employment of Co Nonsolvency of PNIPAM brushes. *Polymer* **2016**, *102*, 372–378.

(4) Liu, Y.; Tas, S.; Zhang, K.; de Vos, W. M.; Ma, J.; Vancso, G. J. Thermoresponsive Membranes from Electrospun Mats with Switch able Wettability for Efficient Oil/Water Separations. *Macromolecules* **2018**, *51*, 8435–8442.

(5) Li, D.; Xu, L.; Wang, J.; Gautrot, J. E. Responsive Polymer Brush Design and Emerging Applications for Nanotheranostics. *Adv. Healthc. Mater.* **2021**, *10*, 2000953.

(6) Víšová, I.; Smolková, B.; Uzhytchak, M.; Vrabcová, M.; Zhigunova, Y.; Houska, M.; Surman, F.; de los Santos Pereira, A.; Lunov, O.; Dejneka, A.; Vaisocherová Lísalová, H. Modulation of Living Cell Behavior with Ultra Low Fouling Polymer Brush Interfaces. *Macromol. Biosci.* **2020**, *20*, 1900351.

(7) Daniel, D.; Goh, S. S.; Truong, T. N. B.; Koh, X. Q.; Tomczak, N. Origin of Underwater Oil Repellence in Polyelectrolyte Brush Surfaces. *Adv. Mater. Interfaces* **2021**, *8*, 2001203.
(8) Horst, R. J.; Pérez, M. B.; Cohen, R.; Cirelli, M.; Robles, P. S. D.; Elshof, M. G.; Andreski, A.; Hempenius, M. A.; Benes, N. E.; Daman, C.; de Beer, S. Swelling of Poly(methyl acrylate) Brushes in Acetone Vapor. *Langmuir* **2020**, *36*, 12053−12060.
(9) Rosenthal, A.; Mantz, A.; Nguyen, A.; Bittrich, E.; Schubert, E.; Schubert, M.; Stamm, M.; Pannier, A. K.; Uhlmann, P. Biofunction alization of Titanium Substrates Using Nanoscale Polymer Brushes with Cell Adhesion Peptides. *J. Phys. Chem. B* **2018**, *122*, 6543−6550.
(10) Adam, S.; Koenig, M.; Rodenhausen, K. B.; Eichhorn, K. J.; Oertel, U.; Schubert, M.; Stamm, M.; Uhlmann, P. Quartz Crystal Microbalance with Coupled Spectroscopic Ellipsometry Study of Temperature Responsive Polymer Brush Systems. *Appl. Surf. Sci.* **2017**, *421*, 843−851.
(11) Yong, H.; Bittrich, E.; Uhlmann, P.; Fery, A.; Sommer, J. U. Co Nonsolvency Transition of Poly(N isopropylacrylamide) Brushes in a Series of Binary Mixtures. *Macromolecules* **2019**, *52*, 6285−6293.
(12) Bünsow, J.; Kelby, T. S.; Huck, W. T. S. Polymer Brushes: Routes towards Mechanosensitive Surfaces. *Acc. Chem. Res.* **2010**, *43*, 466−474.
(13) Schubotz, S.; Honnigfort, C.; Nazari, S.; Fery, A.; Sommer, J. U.; Uhlmann, P.; Braunschweig, B.; Auernhammer, G. K. Memory Effects in Polymer Brushes Showing Co Nonsolvency Effects. *Adv. Colloid Interface Sci.* **2021**, *294*, 102442.
(14) Daniel, D.; Ting Chia, A. Y.; Hui Moh, L. C.; Liu, R.; Koh, X. Q.; Zhang, X.; Tomczak, N. Hydration Lubrication of Polyzwitter ionic Brushes leads to nearly Friction and Adhesion Free Droplet Motion. *Commun. Phys.* **2019**, *2*, 105.
(15) Wetzler, S. P.; Miller, K. A.; Kisley, L.; Stanton, A. L. D.; Braun, P. V.; Bailey, R. C. Real Time Measurement of Polymer Brush Dynamics Using Silicon Photonic Microring Resonators: Analyte Partitioning and Interior Brush Kinetics. *Langmuir* **2020**, *36*, 10351−10360.
(16) Yu, Y.; Kieviet, B. D.; Liu, F.; Siretanu, I.; Kutnyanszky, E.; Vancso, G. J.; de Beer, S. Stretching of Collapsed Polymers causes an Enhanced Dissipative Response of PNIPAM Brushes near their LCST. *Soft Matter* **2015**, *11*, 8508−8516.
(17) Sui, X.; Chen, Q.; Hempenius, M. A.; Vancso, G. J. Probing the Collapse Dynamics of Poly(*N* isopropylacrylamide) Brushes by AFM: Effects of Co Nonsolvency and Grafting Densities. *Small* **2011**, *7*, 1440−1447.
(18) Wang, T.; Yu, Y.; Chen, D.; Wang, S.; Zhang, X.; Li, Y.; Zhang, J.; Fu, Y. Naked Eye Plasmonic Indicator with Multi Responsive Polymer Brush as Signal Transducer and Amplifier. *Nanoscale* **2017**, *9*, 1925−1933.
(19) Ionov, L.; Sapra, S.; Synytska, A.; Rogach, A. L.; Stamm, M.; Diez, S. Fast and Spatially Resolved Environmental Probing Using Stimuli Responsive Polymer Layers and Fluorescent Nanocrystals. *Adv. Mater.* **2006**, *18*, 1453−1457.
(20) Guan, G.; Wu, M.; Han, M. Y. Stimuli Responsive Hybridized Nanostructures. *Adv. Funct. Mater.* **2020**, *30*, 1903439.
(21) Tang, C.; Feng, H.; Huang, Y.; Qian, Z. Reversible Luminescent Nanoswitches Based on Aggregation Induced Emission Enhancement of Silver Nanoclusters for Luminescence Turn on Assay of Inorganic Pyrophosphatase Activity. *Anal. Chem.* **2017**, *89*, 4994−5002.
(22) Rauch, S.; Eichhorn, K. J.; Oertel, U.; Stamm, M.; Kuckling, D.; Uhlmann, P. Temperature Responsive Polymer Brushes with Clicked Rhodamine B: Synthesis, Characterization and Swelling Dynamics Studied by Spectroscopic Ellipsometry. *Soft Matter* **2012**, *8*, 10260.
(23) Tas, S.; Kopeć, M.; van der Pol, R.; Cirelli, M.; de Vries, I.; Bölükbas, D. A.; Tempelman, K.; Benes, N. E.; Hempenius, M. A.; Vancso, G. J.; de Beer, S. Chain End Functionalized Polymer Brushes with Switchable Fluorescence Response. *Macromol. Chem. Phys.* **2019**, *220*, 1800537.
(24) Kopec, M.; Tas, S.; Cirelli, M.; van der Pol, R.; de Vries, I.; Vancso, G. J.; de Beer, S. Fluorescent Patterns by Selective Grafting of a Telechelic Polymer. *ACS Appl. Polym. Mater.* **2019**, *1*, 136−140.
(25) Kopeć, M.; Pikiel, M.; Vancso, G. J. Surface Grafted Polyacrylonitrile Brushes with Aggregation Induced Emission Proper ties. *Polym. Chem.* **2020**, *11*, 669−674.
(26) Besford, Q. A.; Yong, H.; Merlitz, H.; Christofferson, A. J.; Sommer, J. U.; Uhlmann, P.; Fery, A. FRET Integrated Polymer Brushes for Spatially Resolved Sensing of Changes in Polymer Conformation. *Angew. Chem., Int. Ed. Engl.* **2021**, *60*, 16600−16606.
(27) Lin, F.; Zhang, C.; Du, M.; Wang, L.; Mai, Z.; Chen, T. Superior Robustness of ExEm spFRET to IIem spFRET Method in Live Cell FRET Measurement. *J. Microsc.* **2018**, *272*, 145−150.
(28) Chong, Y. K.; Moad, G.; Rizzardo, E.; Thang, S. H. Thiocarbonylthio End Group Removal from RAFT Synthesized Polymers by Radical Induced Reduction. *Macromolecules* **2007**, *40*, 4446−4455.
(29) Brittain, W. J.; Minko, S. A Structural Definition of Polymer Brushes. *J. Polym. Sci. A Polym. Chem.* **2007**, *45*, 3505−3512.
(30) Penzkofer, A.; Lu, Y. Fluorescence Quenching of Rhodamine 6G in Methanol at High Concentration. *Chem. Phys.* **1986**, *103*, 399−405.
(31) Arbeloa, F.L.; Ojeda, P.R.; Arbeloa, I.L. Fluorescence Self Quenching of the Molecular Forms of Rhodamine B in Aqueous and Ethanolic Solutions. *J. Lumin.* **1989**, *44*, 105−112.
(32) Setiawan, D.; Kazaryan, A.; Martoprawiro, M. A.; Filatov, M. A First Principles Study of Fluorescence Quenching in Rhodamine B Dimers: How can Quenching occur in Dimeric Species? *Phys. Chem. Chem. Phys.* **2010**, *12*, 11238−12244.
(33) Egbaria, K.; Friedman, M. Adsorption of Fluorescein Dyes on Albumin Microspheres. *Pharm. Res.* **1992**, *9*, 629−635.
(34) Ritsema van Eck, G. C.; Veldscholte, L. B.; Nijkamp, J.; de Beer, S. Sorption Characteristics of Polymer Brushes in Equilibrium with Solvent Vapors. *Macromolecules* **2020**, *53*, 8428−8437.
(35) Yong, H.; Rauch, S.; Eichhorn, K. J.; Uhlmann, P.; Fery, A.; Sommer, J. U. Co nonsolvency Transition of Polymer Brushes: A Combined Experimental and Theoretical Study. *Materials (Basel)* **2018**, *11*, 991.
(36) Kremer, K.; Grest, G. S. Dynamics of Entangled Linear Polymer Melts: A Molecular Dynamics Simulation. *J. Chem. Phys.* **1990**, *92*, 5057.
(37) Plimpton, S. Fast Parallel Algorithms for Short Range Molecular Dynamics. *J. Comput. Phys.* **1995**, *117*, 1−19.